Final Draft

of the original manuscript

Zhang, W.; Xiong, P.; Meng, Q.; Dudzinska-Nowak, J.; Chen, H.; Zhang, H.; Zhou, F.; Miluch, J.; Harff, J.:

Morphogenesis of a late Pleistocene delta off the south-western Hainan Island unraveled by numerical modeling.

In: Journal of Asian Earth Sciences. Vol. 195 (2020) 104351.

First published online by Elsevier: 10.04.2020

https://dx.doi.org/10.1016/j.jseaes.2020.104351

Morphogenesis of a late Pleistocene delta off the south-western Hainan Island unraveled by numerical modeling

Wenyan Zhang [1,*], Ping Xiong[2], Qicheng Meng[3], Joanna Dudzinska-Nowak[4], Hui Chen[2], Han Zhang[3], Feng Zhou[3], Jakob Miluch[4] and Jan Harff [4]

[1] *Institute of Coastal Research, Helmholtz-Zentrum Geesthacht, Max-Planck-Strasse 1, 21502 Geesthacht, Germany*
[2] *College of Marine Science and Technology, China University of Geosciences (CUG), Wuhan, 430074, China*
[3] *State Key Laboratory of Satellite Ocean Environment Dynamics, Second Institute of Oceanography, Ministry of Natural Resources, Hangzhou, China*
[4] *Institute of Marine and Coastal Sciences, Faculty of Geoscience, University of Szczecin, ul. A. Mickiewicza 18, 70-383 Szczecin, Poland*

[*] Corresponding author: wenyan.zhang@hzg.de, Tel: +49 (0)4152 87 1568

Abstract

A paleo-river delta off the south-western (SW) Hainan Island has been identified based on seismic and core evidence. Dating results suggest its initial development in ~65 kyr BP during a global sea level lowstand (~85 m below modern level) and termination in ~56 kyr BP during a sea level highstand (~50 m below modern level). Analysis of the delta internal architecture indicated a dominant offshore transport pathway from the SW Hainan Island. In order to unravel possible driving mechanisms for morphogenesis of the delta, 3-Dimensional numerical modeling was applied to investigate oceanographic and morphodynamic scenarios corresponding to the initial delta development. Results indicate that sediment dynamics in the study area is controlled by a compound effect of monsoon-driven circulation, river plumes, tides and typhoons. Contribution of the Red River to the delta development is smaller than local rivers in SW Hainan due to a combined effect by regional circulation and tides which causes a detour of the buoyancy-driven plume around the delta, despite of its larger runoff and sediment discharge compared to those from the local rivers of Hainan. On the other hand, simulation results suggest at least ten-times higher sediment supply rate from SW Hainan during the developing phase of the river delta than the modern condition. Such enhanced sediment supply might be caused jointly by 1) increased local river runoff from SW Hainan,

and 2) alongshore transport from eastern Hainan which was connected to the main land during the sea level lowstand.

Keywords: sediment transport; sea level change; coastal morphodynamics; regional circulation; tides; typhoons

---

1. Introduction

River deltas are coastal landforms created by dynamic interactions between terrestrial output of water and sediment, and oceanic forcing including tides, wind waves, storm surges, and mean sea-level variations. A prerequisite for delta formation is that the depositional rate of river-borne sediment exceeds the erosional rate caused by oceanic forcing that carries sediment away from the river mouth, so that net sediment accumulation occurs directly off the river mouth and feeds a growth of the sedimentary system. Depending on different combinations of river-borne sediment supply, tidal amplitudes and wind-wave strength, delta morphology can be in general classified into three types, namely river-dominated, tide-dominated and wave-dominated (Galloway, 1975). Later, this tripartite scheme was extended by Orton and Reading (1993) to include sediment grain size as a fourth principal axis. This classic classification has provided a simple conceptual basis for categorizing river deltas worldwide. However, it is also worth to note that each of the four controlling factors (sediment property, river runoff, tides and wind-waves) may vary considerably over space and time even in the same delta system (Anthony, 2015), furthermore, complicated geological or morphological boundary constraints may also substantially modify the interactions between the fluvial and oceanic forcing (e.g. Wu et al., 2010). Another fact is that although river-borne sediment is the primary source for most river deltas, exogenous sediment transported alongshore by currents or derived from the inner shelf by wave reworking may also contribute significantly to delta development (Anthony, 2015). Therefore, it is important to understand the morphological development of river deltas from a dynamic point of view, and acknowledge that the attributes of each river delta may deform through a wide range of processes that act across multi-scales (Swenson et al., 2005; Geleynse et al., 2011; Hoitink et al., 2017).

Over a longer time scale (centennial-to-millennial), impact of climate change on river discharge and mean sea level causes river deltas to be in a state of transition, e.g. from transgression to regression or vice versa. The resilience of river delta development to a changing climate greatly depends on the sediment supply in relation to sea-level change and the ecological function within the delta system (e.g. vegetation growth) (Besset et al., 2019). A reduction or cut-off of sediment supply would lead to erosion of river delta until it is completely abandoned. Examples of abandoned delta lobes can be seen at the Mississippi River where at least five distinct abandoned delta lobes have been created during the past 6000 years due to relocation of the main river channel (Blum and Roberts, 2012), and at the northern Jiangsu coast where an abandoned Yellow River delta (developed between 1128 and 1855 AD) is located more than 400 km away from its current river mouth (Xue, 1993).

Recently, an abandoned river delta, with an area exceeding 25,000 km^2 and being buried beneath modern coastal deposits, has been discovered off the SW Hainan Island (Fig. 1) based on seismic and core evidence (Chen et al., 2016a; Feng et al., 2018; Xiong et a., this issue; Miluch et al., this issue). Dating results suggest that the development of the river delta initiated in around 65 kyr BP when the global sea level was at a lowstand (~85 m below modern level) and terminated in around 56 kyr BP when the global sea level was at around a highstand (~50 below modern level) (Waelbroeck et al., 2002; Feng et al., 2018; Xiong et a., this issue). The isopach map of the delta deposit estimated from the seismic data indicates two locally confined depocenters with thickness larger than 50 m in the eastern and western part of the delta, respectively (Fig. 2). Although both depocenters have similar maximum thickness of around 80 m, the eastern one has a larger spatial coverage. Seismic data show general progradational configurations towards the SW, S and SE (Fig.1c), suggesting an offshore expansion during the delta development (Chen et al., 2016a; Feng et al., 2018; Miluch et al., this issue). The onshore and offshore edges of the delta are located at modern water depth of ~50 and ~200 m, respectively.

A set of geomorphic features, including the detachment of the delta from its potential sources, its burial beneath modern sediment deposits, the existence of two locally confined depocenters and their asymmetry in volume and spatial coverage, imposes challenges for a comprehensive understanding of the delta morphogenesis and its associated source-to-sink transport pathways. Furthermore, the runoff and sediment discharge rate of major local rivers in south Hainan are relatively small in modern time (Milliman and Farnsworth, 2011; Yang et al., 2013). The Changhua River and the Wanquan River are two dominant rivers in south Hainan (Fig. 1b) and contribute to ~80% and ~85% of the regional budget of discharge in the south-western and south-eastern part, respectively. The multi-year mean values of river runoff and sediment discharge are $\sim 5 \times 10^9$ m^3 yr^{-1} and $\sim 0.8 \times 10^6$ t yr^{-1} in Changhua River, and $\sim 6.6 \times 10^9$ m^3 yr^{-1} and $\sim 0.6 \times 10^6$ t yr^{-1} in Wanquan River, respectively (Yang et al., 2013). Such values, especially the sediment discharge rates (a total of $\sim 1.8 \times 10^6$ t yr^{-1} from all major rivers in south Hainan in modern time), are too small to account for the average accumulation rate ($\sim 3 \times 10^8$ t yr^{-1} between 65 and 56 kyr BP, Miluch et al., this issue) in the paleo-delta. Therefore, understanding of the morphogenesis of the delta and its sediment sources, associated transport and sedimentation processes remains largely speculative with various knowledge gaps to fill.

Based on existing data derived from an international research project "ERES: Evolution of the "Hainan Delta" as response to the palaeo-environment since the Late Pleistocene at the SCS northwestern shelf", this study aims to explore possible physical driving mechanisms for the morphogenesis of the paleo-river delta by the use of 3-Dimensional process-based numerical modeling. In particular, we seek to identify potential sediment sources for the delta and associated transport patterns in order to fill at least part of the gap in sediment budget. The results will help to advance our understanding of source-to-sink transport in river delta systems and the role of climate change in determining the fate of river deltas.

2. Material and methods

2.1 Study area

The Hainan Island is located in northern South China Sea and geographically separated from the mainland by a narrow strait (Fig. 1). The landscape of Hainan comprises mountains in the central part with height up to 1867 m (above the mean sea level), numerous hills over the entire island and relatively small low-land coastal areas characterized by a series of highly indented promontory embayments. The mountains and hills are mostly composed of Palaeozoic metamorphic and sedimentary rocks intruded by Palaeozoic and Mesozoic granites (Wang et al., 1991). The sandy embayment coast of southern Hainan Island mainly consists of (i) drowned valleys bounded by steep bedrock hills and only locally receiving sediments, (ii) alluvial-deltaic deposits, and (iii) beach ridges/barriers and associated elongated lagoons (Wang, et al., 2001).

Except for the northern part of Hainan that is affected by a humid and subtropical climate, the major part of Hainan is dominated by the tropical monsoon, with north-easterly winds in winter (November to March) and south-westerly winds in summer (May to September) and a transition between the two monsoonal winds in April and October (Zhang et al., 2013). Tropical storms and typhoons frequently (up to 10 times per year) strike the island in every year between June and September, and bring large amounts of rainfall (up to 500 mm per event), accounting for 70% of the annual precipitation (Committee of Encyclopedia of Hainan, 1999). The seasonal monsoon and extreme events largely control the temporal variability of river output to the shelf sea, with 80-85% of annual runoff and sediment discharge occurring between June and October (Yang et al., 2013). Because of a short excursion course (< 350 km) and large elevation difference between the river source in mountains and the river mouth, most major rivers on Hainan are characterized by a relatively large slope, thus facilitating sediment output to the coastal area. Concentrations of 50-200 mg L^{-1} for suspended particulate matter (SPM) are typical for Hainan rivers (Zhang e al., 2013), with higher values for bedload transport. However, a net decreasing trend of sediment discharge is clearly seen during the past decades, mainly due to anthropogenic activities including dam constructions, sand mining and agriculture irrigation (Yang et al., 2013). It is estimated that sediment discharge in major rivers has been reduced by more than 50% since late 1950s (Yang et al., 2013).

Hydrodynamics in the coastal area of Hainan Island is subject to the impact of mixed diurnal and semi-diurnal tides with average tidal ranges between 1.1 and 2 m along the north and north-western coast and below 1 m along the south and south-eastern coast (Li et al., 2019). The wind-waves are relatively weak, with average height less than 1 m along the entire coast (Wang et al., 2001). Besides the impact of astronomical tides, coastal currents are significantly controlled by the monsoon which shows distinct patterns between winter and summer (Liu et al., 2008). Maximum current velocity exceeds 50 cm/s along the south coast as a combined effect of tides and winds (Hu et al., 2003; Gan et al., 2006).

2.2 Reconstruction of the paleo-Digital Elevation Model (DEM)

The coastal morphology in the initial stage (65 kyr BP) of the delta development needs to be approximated before a numerical modelling of the paleo-oceanographic conditions and sedimentation processes. A detailed reconstruction of the paleo-DEM of the study area is described in Xiong et al. (this issue) with similar methods and procedures demonstrated in Zhang et al. (2014). A brief introduction is provided here.

A high-resolution DEM of the coastal area of south-west Hainan extrapolated from densely distributed seismic profiles and multi-beam data was integrated into the latest General Bathymetric Chart of the Oceans (GEBCO) dataset, which has a 30 arc-second resolution (GEBCO_2014, v. 2014-11-03, http://www.gebco.net) to produce a complete modern DEM of the study area (Fig.1b). This DEM served as a starting point for reconstruction of the paleo-DEM. The reconstruction included a reversal of eustatic sea level, i.e. lowering the sea level by 85 m from the modern one (Fig. 3a) according to Waelbroeck et al. (2002), and a removal ("backstripping", Xiong et al., this issue) of the sediment deposit layer after 65 kyr BP. A continuous reflection surface named R2 in the seismic profiles (Fig. 1c) has been found to mark the interface between the river delta and its underlying seafloor (Feng et al., 2018). Sediment deposit above R2 was therefore removed in the reconstruction. After these two procedures, the paleo-DEM for the research area in the initial stage of the delta development in 65 kyr BP was reconstructed and shown in Fig. 3c. Tectonic movement and the impact of consolidation were not considered in the reconstruction procedure due to their minor impact (-0.4–0 mm yr^{-1}) (Feng et al., 2018) compared to the sea level change (4–6 mm yr^{-1}, Fig. 3a).

2.3 Numerical modelling

A 3-D morphodynamic numerical model which has been successfully applied to the South China Sea and other coastal shelf seas (Chen et al., 2016b; Zhang et al., 2016; Chen et al., 2019; Yin et al., 2019) was applied in this study. The model contains four major functional modules: (a) A 3-D circulation module based on the Princeton Ocean Model (Blumberg and Mellor, 1987; Mellor, 2003) adopting a fourth-order vertical pressure gradient scheme from Mccalpin (1994) to better resolve hydrodynamics over complex topography characterised by a sharp bathymetric gradient such as seamounts and continental slope; (b) A bottom boundary layer (BBL) module based on the Styles-Glenn model (Styles and Glenn, 2000) taking into account the impact of stratification induced by suspended particulate matter (SPM) on the vertical structure of current velocity in the constant stress layer; (c) A subaqueous sediment transport module (Zhang et al., 2011) modified from ECOMSED (HydroQual, Inc., 2002) for a process-based formulation of erosion, suspended load/bed load transport, and deposition of cohesive (one grain-size class) and non-cohesive (one grain-size class) sediment; and (d) A bathymetry update module based on the technique of morphological update acceleration and approaches for maintaining the computational stability (Zhang et al., 2012). The reason for applying morphological update acceleration is to up-scale the morphological evolution in long-term modelling. Specifically, the flow, sediment transport and bed level change are all computed using the same time step and then the calculated bed level change at each time step is multiplied by a factor f (≥ 1), so that after a simulation of one tidal cycle the model has, in fact, produced the morphological change for f tidal cycles. However, spurious oscillations may occur if the value of f is too large, especially for high-energy conditions such as typhoons. To avoid unrealistic spurious oscillation near shocks and discontinuities in the computation, no morphological update acceleration (i.e. $f = 1$) was implemented in the simulation of typhoons, while $f = 3$ was used in simulation of normal conditions using the seasonal mean wind fields and astronomical tides as driving forces. After simulation of one year, the calculated bed level change was multiplied by $f = 10$, so that the morphological change of 10 years was produced. Based on the updated morphology the model simulated hydrodynamics and sediment transport for the next annual cycle (i.e. normal seasonal mean conditions and a representative typhoon). This procedure continued until the long-term simulation was finalized. The method has proven to perform well in modelling long-term development of barrier islands (Zhang et al., 2010, 2014) and mud depocenters (Hanebuth et al., 2015; Chen et al., 2019).

A nested computational grid system was utilized to provide a high-resolution simulation of the study area. In this nested system, an orthogonal rectilinear regional grid covering the entire South China Sea and West Pacific Ocean with a uniform horizontal resolution of 15×15 km was used to provide open boundary conditions for a local grid covering the study area (Fig. 3c) with a high horizontal resolution of 800×800 m. The driving forces for the regional model include the water level (η) and flow velocity (u, v) at three open boundaries using the climatology of HYCOM+NCODA Global 1/12°Analysis from 2009 to 2016 (GLBa0.08, https://hycom.org/dataserver/gofs-3pt0/analysis). Four major tidal constituents (M2, S2, K1, O1) derived from TPXO 7.2 (Egbert and Erofeeva, 2002) were imposed to η at the open boundaries. These constituents account for more than 95% of the tidal energy in the study area (Hu et al., 2003). In addition, four constant wind fields, each averaged over three months representing a different season based on the climatology (2000−2011) of sea surface winds (0.25°×0.25°) released from the National Oceanic and Atmospheric Administration (NOAA; http://coastwatch.pfeg.noaa.gov/erddap/griddap/), were specified as seasonal surface driving force. Because typhoons play a very important role in sediment resuspension and redistribution in this area, simulation of typhoon impact on development of the paleo-delta was included. In this study we adopted the wind field of a realistic typhoon (Typhoon Ketsana) occurred between 25-30 September 2009 (JTWC; www.metoc.navy.mil/jtwc/jtwc.html?western-pacific) to simulate the typhoon impact on hydrodynamics and sediment transport. The reason for choosing this typhoon as annual representative extremes in our modelling is that 1) its track followed almost a straight line at the latitude of ~15.5°, which is the lower boundary of our local model domain, and thus had strongest impact in terms of winds and waves in our study area, and 2) it is a Category 2 typhoon with peak wind speed of ~42 m s^{-1}, neither too strong nor too weak, thus could represent annual typhoon conditions in the study area.

A detailed model setup and validation against observational data have been described in Chen et al. (2019). In the modeling of paleo-oceanographic and morphodynamic scenarios corresponding to the initial stage of the delta development, we replaced the modern DEM with the reconstructed paleo-DEM in 65 kyr BP and adopted the same driving forcing as modern time.

Because we are interested in identifying the potential sediment sources, especially the river sources for the delta and associated transport pathways, and for the sake of modelling simplification, only four major rivers in the area, namely the Red River, the Nanliu River, the Changhua River and the Wanquan River (Fig. 3c), are considered in the simulation. Location of each of the river mouths at 65 kyr BP (Fig. 3c) was set based on the paleo-valley axes identified from seismic data (Xiong et al., this issue). Values of river runoff and sediment discharge observed in modern time suggest the Red River as the dominant river supply of the Beibu Gulf, being 10 times of the Nanliu River, 17 times of the Wanquan River and 22 times of the Changhua River in terms of annual mean runoff, and with even higher ratios in total sediment discharge (Table 1). The river boundary outputs in the model are distinguished into two seasonal conditions. Multi-year mean values are used to parameterize the boundary condition in the dry season from December to May, whereas in the wet season (June - November) river runoff is doubled in all rivers, and sediment concentration is increased correspondingly with a higher ratio in the Hainan rivers due to their large bed slope effect (Zhang et al., 2013).

The seafloor is assumed to be free of mobile sediments except for those from the rivers. Two sediment types, namely SPM in the form of suspended load and medium sand in the form of bedload, are specified in the river boundary. A constant value of 0.1 Pa is assumed as the critical shear stress for re-suspension of unconsolidated sediment. A lower value (0.03 Pa) is used as the critical shear stress for sediment deposition. Setting of these two values is based on recommended values for sand-mud mixture bed conditions by van Rijn (2007). Sensitivity tests by varying these two critical thresholds by $\pm 30\%$ indicate minor differences in the resultant erosion/deposition pattern in our study area.

3. Results

3.1 Hydrodynamics

3.1.1 Hydrodynamics in normal conditions

Simulation results reveal that the regional circulation, especially along the shelf edge, is largely driven by the monsoon system, whereas the coastal shelf circulation is predominantly controlled by astronomical tides with significant modulation by the monsoon and buoyancy-driven river plumes from the major rivers (Figs. 4, 5). The compound effect of tides, river runoff and winds results in distinct transport patterns between winter and summer seasons, as well as asymmetry in current strength between the eastern (i.e. Hainan) and western coast (i.e. Vietnam).

In winter, currents outside the embayment as well as along the south-eastern coast of Hainan are mainly driven by the north-easterly winds. The flood tides further enhance the current strength along the south-eastern Hainan coast, resulting in peak velocities up to 1 m s^{-1} in surface layer and ~0.4 m s^{-1} near the bottom around the southern tip of Hainan (Fig. 4a, b). In contrast to energetic hydrodynamic regime along the Hainan coast, the western coast of the embayment is calm during the flood tides, with current velocity below 0.2 m s^{-1} along its major part except for a local enhancement (0.4-0.5 m s^{-1}) at the paleo-Red River mouth (Fig. 4a). This local enhancement of current velocity is seen in the surface water only, indicating that it is associated with the buoyancy-driven river plume. During the ebb phase, strong currents are seen along the coast on both sides of the embayment (Fig. 5a, b). Due to the impact of monsoon, currents along the south-eastern Hainan coast are directed south-westwards even during the ebb tides. As consequence, the ebb tidal outflow is pushed toward the western coast (Vietnam) and in the meanwhile spatially enhanced, with surface current velocity up to 0.6 m s^{-1} in various parts along the western coast (Fig. 5a, b).

In summer, the south-westerly winds drive the surface currents north-eastwards along both the shelf edge and the south-eastern coast of Hainan. During the flood tides, such currents counteract the tidal current along the south-eastern coast of Hainan, resulting in a relatively weak hydrodynamic regime in this local area (Fig. 4c, d), whereas in a major part of the embayment a superposition of the wind-driven circulation and the tidal current results in high flow velocities (>0.5 m s^{-1} in surface water) there. During the ebb phase, the tidal outflow converges with the wind-driven outer-shelf currents at the southern tip of Hainan, resulting in peak velocities up to 0.9 m s^{-1} in surface water (Fig. 5c, d). In contrast to the high current velocity along the Hainan coast, the western coast of the embayment is relatively calm during the ebb tides, with current velocity below 0.2 m s^{-1} along its major part except for a local enhancement (0.4-0.5 m s^{-1}) at the paleo-Red River mouth. This situation is similar to that during the flood tides in winter season, but with a difference in the transport pathway of the Red River plume (Fig. 4a, Fig. 5c).

Dispersal of the buoyancy-driven river plumes is reflected from the salinity distribution in the study area (Fig. 6). In dry season, the Red River plume is confined along the western coast of the embayment and transported southwards along the coastline (Fig. 6a, b). The north-easterly winds pushes the surface water towards the western coast and results in prominent downwelling there. As a consequence, part of the fresh water from the Red River plume is transported downwards. A density front is formed between the downwelling light (1015-1021kg m^{-3}) water from the Red River and the dense (1025 kg m^{-2}) ambient marine water, which further confines the offshore extension of the riverine water and in the meanwhile enhances the alongshore transport speed of the river plume. In contrast to the prominent Red River plume, the plumes from the other three rivers are limited to local areas around the river mouths due to small runoff values. In wet season characterized by greatly enhanced river runoff and reversed wind direction, the Red River plume no longer follows the western coastline of the embayment. Instead, it is transported towards the eastern coast and converges with the Nanliu River plume (Fig. 6c, d). The converged plume is further transported south-eastwards along the Hainan coast and joins the Changhua River plume. The reinforced plume separates into two branches after bypassing the southern tip of Hainan, with one of them following still the coastline and transported north-eastwards and the other heading for the open ocean towards the shelf break. It is worth to note that downwelling and strong mixing occur in the northern part of the embayment near the Nanliu River mouth, causing a wide spread of less saline water all though the water column in this area (Fig. 6d), whilst downwelling is weakened in the mid-way between the Nanliu River and the Changhua River and at some local places replaced by weak upwelling. As a result the less saline water in the bottom layer (originated from the rivers) is confined in a narrow zone along the coastline along the transport path of the surface river plume.

The dynamic interaction between the large-scale monsoon-driven circulation, the buoyancy-driven river plumes and the tidal currents has a dominant control of the net transport (averaged over 120 tidal cycles, Fig. 7).

In dry season (December - May), a strong south-westward transport exists along the south-eastern coast of Hainan (Fig.7a). The residual current velocity reaches up to 0.5 m s^{-1} along this part of coast. This energetic transport terminates after bypassing the southern tip of Hainan and entering the embayment. In contrast to the south-eastern coast, the western coast of Hainan is characterized by a weak residual transport (<0.05 m s^{-1}), with only local enhancement (0.05-0.1 m s^{-1}) associated with the river run-off from the Nanliu and Changhua Rivers. A net southward transport of the Changhua River runoff is seen, and it converges further offshore with the strong south-westward transport along the south-eastern Hainan coast. A relatively strong southward transport (with residual current velocity of 0.1-0.3 m s^{-1}) originating from the Red River mouth also occurs along the western coast of the embayment. It is a result of the Red River plume transport confined by the density front (Fig. 6a,b).

In wet season (June - November), the strong residual transport along the south-eastern Hainan coast is reversed (Fig. 7b). The southward transport along the western coast of the embayment in dry season ceases in wet season. A net transport, characterized by residual current velocity of 0.1-0.2 m s^{-1}, occurs from the Red River mouth towards the Changhua River mouth and is associated with dispersal of the buoyancy-driven river plume (Fig. 6c, d).

Besides the above-mentioned residual transport patterns along the coast, cyclonic and anti-cyclonic gyres occur in various parts of the embayment (Fig. 7). The areas off the Red River mouth and the Changhua River mouth appear to be hotspots of gyres that persist over different seasons with certain spatial oscillations.

3.1.2 Hydrodynamics during typhoons

Hydrodynamics in the study area become quite energetic during typhoons (Fig. 8). Surface water is pushed by strong south-easterly winds towards the embayment head where the Red River and the Nauliu River are located. Maximum current velocity reaches up to 1 m s^{-1} along both edges of the embayment. The piling up of water at the embayment head results in a south-eastward compensation flow in the middle part of the embayment. This compensation flow is characterized by relatively weak surface currents (<0.3 m s^{-1}) but quite strong bottom currents (0.3-0.6 m s^{-1}) (Fig. 8b). The modelled maximum significant wave height is ~10 m at the shelf break (200 m water depth), and gradually decreased to ~3.5 m at the Red River mouth. A combination of strong waves and currents results in large bottom shear stress (between 1 and 10 Pa) over a major part of the embayment that well exceeds the threshold for resuspension of unconsolidated surface sediments (0.1 Pa).

3.2 Sediment dynamics and morphological change

3.2.1 Normal conditions

The transport of suspended sediment (i.e. SPM) from the major rivers, as illustrated in Fig.9, shares similarity as well as difference with that of the buoyancy-driven river plume shown in Fig.6. In general, the major transport pathway of SPM follows that of the river plume (Fig. 9a, b), on the other hand, deposition and resuspension cause also significant deviation in the transport of sediment from the river plume.

In dry season, SPM from the Nanliu and Changhua Rivers is transported mainly offshore towards the western coast of the embayment (Fig. 9a). Deposition and resuspension occur along its transport path due to alternating hydrodynamic regimes controlled by tides and winds. As a result, river-borne fine-grained sediment is spread over a major part of the embayment in the bottom layer (Fig. 9b). In contrast to the offshore transport pattern from the Nanliu and Changhua Rivers, transport of SPM originated from the Red River and the Wanquan River is mainly confined along the coastline. The most prominent transport is from the Red River which is the main supplier of both fresh water and sediment. Massive deposition and resuspension occur along the western coast of the embayment following the pathway of the Red River plume. However, spread of the resuspended sediment originated from the Red River is also spatially confined near the western coast. It is worth to note that although the sediment discharge from the Wanquan River takes up only a very small portion of the total river-borne sediment input rate in the study area, a net transport along the south-eastern Hainan coast towards the embayment is seen in the bottom layer (Fig. 9b). This pattern indicates that fine-grained sediment from the Wanquan River goes through numerous cycles of deposition, resuspension and near-bottom transport before reaching the paleo-river delta area. The simulated depositional thickness after a dry season indicates that the major deposition occurs in water depth between 20 and 50 m along the western coast of the embayment, with a maximum thickness of ~0.3 cm (Fig. 10a). A thin layer of deposit (~0.1 cm) occurs along the western Hainan coast and its sediment source is mainly from the Nanliu and Changhua Rivers. In the paleo-delta area, only the western part receives deposited sediment with a major portion coming from the Red River, whereas the eastern part is free of deposition due to insufficient sediment supply from the eastern Hainan coast. A thin belt of deposit (~0.1 cm) is formed by sediment discharge from the Wanquan River, and extends towards the delta area.

In wet season, fine-grained sediment from the Nanliu and Red Rivers is mainly accumulated in the northern part of the embayment (Fig.9c, d). In energetic hydrodynamic conditions, freshly-deposited river-borne sediment in this area is re-suspended again and partly transported south-eastwards along the western Hainan coast. Unlike the river plume which separates into two branches after bypassing the southern tip of Hainan, SPM is mainly confined in the branch along the coast and transported towards northeast. Massive resuspension induced by periodic strong tidal currents facilitates an offshore spread of the river-borne sediments in the bottom layer (Fig.9d). The simulated depositional thickness after a wet season indicates a quite different pattern with that after a dry season (Fig. 10). Remarkable deposition (maximum thickness of ~0.8 cm) occurs in the northern part of the embayment, especially off the Red and Nanliu River mouths, due to accumulation of sediment from these two rivers. The deposition extends south-eastwards with much reduced thickness (~0. 1 cm) and connects to a depocenter off the Changhua river mouth. A maximum depositional thickness of ~0.4 cm is simulated in the depocenter. Its direct connection to the Changhua River mouth with increased depositional thickness indicates that the major sediment source is from this river. An alongshore extension of the deposit suggests that the other three rivers may also contribute to its formation to some extent.

3.2.2 Typhoon impact

The typhoon-induced strong bottom currents, which follow the geometry of the Yinggehai Basin (Fig. 8), provide a highly effective means for sediment delivery from the Red River mouth towards the deeper Yinggehai Basin and the shelf break (Fig. 11). Massive resuspension of the freshly deposited sediment after the wet season (Fig. 10b) occurs due to greatly enhanced bottom shear stress caused by a combined action of strong currents and waves, with most remarkable effect off the Red River mouth (Fig. 11a). The resuspended sediment is mostly entrained by the bottom currents and transported towards the deeper Yinggehai Basin and the outer shelf, forming a belt-line deposit in the Yinggehai Basin after the typhoon (Fig. 11b). On the other hand, the typhoon causes significant erosion along the coastline with most severe impact on the depocenter off the Red River mouth. A comparison between the deposited volume in normal conditions (Fig. 10) and erosion by the typhoon (Fig. 11b) indicates that about 50% of the freshly deposited sediment (e.g. on the depocenter off the Red River mouth) is remobilized and transported to the Yinggehai Basin within a year.

3.2.3 Long-term results

The iteration of the two distinct seasonal transport patterns including their transition and typhoons re-organizes the distribution of sediment deposition on a longer time scale. Simulated depositional thickness after 50 yrs since the onset of modeling indicates that two large-scale deposits are created by the river discharge (Fig. 12a). One is centered in the northern part of the embayment and results mainly from the Red River discharge. The other is located off the Changhua River mouth and exhibits a fan shape, with maximum deposition near the river mouth. These two large-scale deposits are connected through three belts, with two thin ones at each side of the embayment respectively and characterized by deposition thickness less than 10 cm and a relatively broad one in the middle (Yinggehai Basin) with thickness between 5 and 15 cm . The existence of these belts suggests three major transport pathways of river-borne sediment from the Red River to the paleo-river delta, with the western one associated with the transport in dry season, the eastern one in wet season and the middle one in typhoons, respectively. A calculation of the total deposited sediment budget in the paleo-river delta area and deposition from each individual river (with sediment discharge from other rivers shut down in simulation) indicates a dominant supply (~55.7%) from the local river, i.e. the Changhua River, with a significant contribution (37.4%) by the Red River, and subordinate contribution by the other two rivers (Fig. 12b).

4. Discussion

4.1 Implication of simulation results

This study aims to explore possible physical driving mechanisms for the morphogenesis of an abandoned paleo-river delta found off SW Hainan Island and to identify potential sediment sources for the delta and associated transport patterns. We are convinced that our simulation results provide useful information to address a major part of these issues.

Our results indicate that in ~65 kyr BP when the global sea level was at a lowstand (~85 m below modern level), the Hainan Island seen today was not an island but part of the mainland, and the Beibu Gulf was an embayment (Fig. 3c). The modern-like monsoon, which has been established since the early Miocene (~ 22 million yr BP; e.g. Clift et al., 2014), produces two distinct large-scale seasonal circulation patterns in the South China Sea. Because of a lowstand of sea level in ~65 kyr BP, a significant part of the continental shelf was emerged. As a result the regional circulation, especially that along the shelf edge and coastal area, was quite energetic at that time (Xiong et al., this issue). The interaction between the monsoon-driven circulation, the astronomical tides and the buoyancy-driven river plumes results in two distinct seasonal transport patterns of river-borne sediment in the embayment and its adjacent area. In addition, frequently-occurred typhoons play an important role in redistribution of freshly deposited sediment in the wet season.

In dry season (December - May), sediment from the Red River, which is a major supplier of both runoff and sediment to the embayment, is mainly transported along the western coast of the embayment and detoured around the paleo-river delta, whereas fine-grained suspended sediment from the Nanliu and Changhua Rivers is transported offshore (Fig. 9b). Such offshore transport direction indicates that sediment from other rivers along the western Hainan coast (Fig. 1b), although not included in our modelling, would be transported similarly, facilitating formation of the paleo-river delta. Satellite images for this region taken in late November 2001, when north-easterly winds dominated, provide support for the offshore transport pattern (Fig. 13). Besides the western Hainan coast, sediment from the south-eastern Hainan coast such as the Wanquan River or even from further remote rivers is also transported towards the paleo-delta in dry season and serves as potentially important source (Fig.9b). The strong coastal currents along the eastern Hainan and the connected mainland coast may effectively transport sediment towards the southern tip of Hainan, where a drastic decrease of current strength occurs, leading to decrease of sediment transport capacity and subsequent deposition there. Various gyres developed as a result of residual transport (Fig. 7a) may further facilitate deposition in the delta area, as evidenced in other regions where some large-scale deposits are associated with persistent gyres (e.g. Sündermann and Pohlmann, 2011; Miramontes, 2019; Zhang et al., 2019). The contribution to sediment budget from the eastern Hainan coast and the connected mainland coast (e.g. from the Pearl River) is heavily underestimated in our model results, in which only the impact of the Wanquan River is taken into account (Fig. 12b).

In wet season (June-November), sediment from the Red River is mainly accumulated near the river mouth due to the existence of several long-lasting gyres there which promotes deposition in their centre (Fig. 7b). Only a small portion (< 5%) of the fine-grained sediment from the Red River is further transported along the western Hainan coast and contributes to development of the delta. Our simulation results indicate that the suspended sediment plumes from the Red and Nanliu Rivers converge with the plume from the local river in SW Hainan, i.e. the Changhua River, before their further dispersal towards the delta front (Fig. 9c, d).

Typhoons frequently occur in the region and may play an important role in re-organizing the deposit patterns, despite of a short period of their direct impact (within a few days). Our results suggest that typhoons are capable of massive resuspension of surface sediments that are freshly deposited in the embayment, and subsequently transport them into the Yinggehai Basin (Fig. 11). These results provide further support that most sediment delivered by the Red River is initially deposited near its river mouth, and then resuspended during high-energy conditions (e.g. during typhoons) and transported into the Yinggehai Basin. Such deposition pattern is supported by existing literature. For example, a seismic profile extending across the Yinggehai Basin including the paleo-Red River mouth provided by Clift and Sun (2006) in their figure 3 shows that the filling of the basin is characterized by a south-westward trend. In addition, the sediment isopach map for the entire Yinggehai Basin from Clift and Sun (2006) does show existence of a depocenter at the paleo-Red River mouth. It is particularly worth to note that although transport of the Red River-borne sediment into the Yinggehai Basin would also promote deposition in the paleo-delta off west Hainan, it is not the formation mechanism of the delta. This is clearly indicated by both model results (Fig. 11) and seismic profiles across the paleo-delta (e.g. Fig. 1c) showing that the internal architecture of the river delta is featured by deltaic deposits mainly fed by sediment from the western Hainan (Chen et al., 2016a; Feng et al., 2018).

The potential of river delta development along the SW Hainan in modern condition has been proposed by Li et al. (2019), who classified the entire Hainan coast into three geomorphological zones, e.g. the northern mixed estuaries zone, the western river deltas zone, and the eastern coastal lagoons zone. This classification is based on analysis of the river-borne sediment supply rates, the estuarine accommodation space and the hydrodynamic forcing. In modern period, various small-scale river deltas are found along the western Hainan coast due to the impact of wind-waves, whereas no delta is formed in the northern or eastern

Hainan coast due to a compound effect of insufficient accommodation space, larger tidal amplitudes and typhoon-induced erosion (Li et al., 2019). If similar setting of monsoon, tides and typhoon is shared in 65 k BP as today, the outcome of Li et al. (2019) implies that under favourable condition in terms of increased sediment supply, large-scale river delta may form in the SW Hainan coast.

4.2 Limitation of simulation results

Although we are able to provide a plausible explanation for morphogenesis of the paleo-river delta off the SW Hainan. Several gaps in understanding still exist. One is that the two locally-confined depocenters in the delta (Fig. 2), especially the one on the eastern side, were not fully reproduced in our model results. We hypothesize that part of the failure is attributed to simplification of sediment sources in the model by considering only four river outputs and neglecting other potentially important sources, especially the connected mainland coast where the Pearl River, the second largest river in terms of mean discharge in China with a multi-year mean value of $\mathbf{\sim 1 \times 10}^4$ m^3 s^{-1}, is located. Because our model results indicate a south-westward extension of the deposit from the Wanquan River mouth toward the eastern depocenter (Figs. 10 and 12), we hypothesize that this depocenter is formed mainly by the transport pattern in dry season and its main source is from the eastern Hainan coast and the connected mainland coast, e.g. the Pearl River. A dominant south-westward transport of Pearl River sediment during lowstand of sea level has been confirmed by Liu et al. (2017). The existence of an elongated mud belt along the western Guangdong coast adjacent to Hainan with identified sediment source from the Pearl River (Liu et al., 2010) provides support for our hypothesis. The western depocenter is likely related to the transport pathways in wet season and during typhoons with its main source from the Red River and the local SW Hainan according to our simulation results. Nevertheless, more evidence in field data is needed to justify our hypothesis on the distinct source-to-sink transport pathways for formation of these two depocenters in the paleo-delta system.

Another gap in understanding is about the sediment budget. The estimated annual-mean sedimentation rate on the paleo-river delta is ~$\mathbf{3} \times \mathbf{10}^8$ t yr^{-1} (Miluch et al., this issue), whilst the modelled sedimentation rate in the delta area is ~ $\mathbf{1.7} \times \mathbf{10}^7$ t yr^{-1}, being one order of magnitude smaller. This inconsistency indicates that the sediment supply rate during the developing phase of the river delta should be at least one order of magnitude higher than modern condition. Based on our simulation results, we hypothesize that such enhanced sediment supply might be caused jointly by 1) increased local river discharge from SW Hainan, and 2) alongshore transport from eastern Hainan which was connected to the main land during the sea level lowstand. The latter has been discussed previously, while the former might probably be caused by enhanced precipitation due to monsoon variation (An, 2000; Li et al., 2019). It is worth to note that the multi-year mean runoff and SPM concentration of four major rivers in modern time were used in this study as reference to parameterize the river discharge and sediment supply for 65-56 kyr BP. These values may fluctuate significantly due to human and climate impacts and therefore would cause errors in our budget analysis. For example, Clift and Sun (2006) found that the average sediment delivery rate from the Red River for the Pleistocene is $\mathbf{4} - \mathbf{6} \times \mathbf{10}^7$ t yr^{-1}, which is less than half of the Holocene condition ($\sim\mathbf{1.3} \times \mathbf{10}^8$ t yr^{-1}). However, although fluctuations exist in the river discharge, there is no doubt that the Red River is the major supply of this region. Therefore, further tuning of the river boundary conditions will not violate the validity of our interpretation on the formation mechanism of the paleo-river delta and source-to-sink sediment transport pathways from the major rivers.

Based on biomarker proxy-data analyses of sediment core samples from the paleo-delta Tomczak et al. (2019, this issue) have reconstructed the SST (Sea Surface Temperature) for the time span 65 kyr BP to 56 kyr BP, i.e. the development period of the Hainan Delta. According to their results the SST dropped at 65 kyr BP before it returned at 61 kyr to warmer conditions. The fall of the temperature at 65 kyr BP coincides with a positive anomaly in the $\delta^{18}O$ record supporting the hypothesis of strengthened winter monsoon at this time. A reanalysis of meteorological data covering 1871-2012 did discover that precipitation at Hainan Island correlates negatively with precipitation over much of the rest of Monsoon-affected Asia, so that strengthened winter monsoon conditions in Asia likely lead to enhanced rainfall rates at Hainan Island (Xiong et al., this issue). As indicated by our simulation results, offshore spread of river-borne sediment from the SW Hainan coast in winter monsoon condition would facilitate the growth of the paleo-delta.

Another issue remaining to be addressed is the cause for termination of the paleo-delta development in ~56 kyr BP. The global sea level was at a highstand (~50 m below modern level) and starting to drop during this period (Waelbroeck et al., 2002, Fig.3a), and Hainan remained connected to the mainland (Xiong et al., this issue). It is known that reduction or cut-off of sediment supply would lead to erosion of river delta (Xue, 1993; Blum and Roberts, 2012). Increase of subaqueous accommodation space induced by sea-level rise that exceeds the sedimentation rate would also lead to delta deterioration. The rising sea level might contribute to delta destruction in our study area, but it should not be the major cause because the development of the delta had been through a more drastic sea-level rise in its initial phase (Fig. 3a). Sediment supply rate was able to outpace the sea-level rise in that period to feed a continuous development of the delta, causing a so-called “normal regression” effect. Therefore, a more plausible explanation is a reduction of sediment supply. Li et al. (2019) reported that discharge of fluvial fine-grained sediment, mainly fine and very fine silts (2-10 μm), along the northern South China Sea coast is mainly controlled by the East Asian summer monsoon precipitation. Cooling climate events led to decrease of the fluvial fine-grained sediment in the coastal shelf deposits, vice versa. Sediment cores derived from the paleo-delta suggest a dominance of fine silts and clay (2-16 μm) taking up more than 90% in the lower delta deposit layer with a general upward coarsening trend (Miluch et al., this issue). Because the following period after 56 kyr BP was characterized by a quick drop of sea level (by ~20 m till 52 kyr BP), which corresponded to a cooling climate and subsequent reduction of summer monsoon precipitation. This implies a drastic reduction of river-borne sediment supply. Furthermore, winter monsoon might also strengthen in cooling climate and lead to stronger coastal currents and wind-waves that erode the river delta. The combined effect of reduction in sediment supply and enhanced erosion in the cooling period between 56 and 52 kyr BP is hypothesized to be the main cause for termination of the delta development.

5. Conclusions

Based on a paleo-DEM of SW Hainan and its adjacent coastal area reconstructed from seismic reflection profiles, sediment cores with dating results and global sea level curve, this study uses 3D process-based numerical modeling to examine how large-scale monsoon-driven circulation, astronomical tides and buoyancy-driven river plumes interact to influence the formation of a paleo-river delta off SW Hainan.

Three major conclusions are drawn from the study. First, the sea level lowstand in ~65 kyr BP imposes a first-order control on the coastline configuration and distribution of available sediment sources for morphogenesis of the delta. Hainan was part of the mainland and the Beibu Gulf was an embayment. The area where the paleo-delta was located acts as a gate connecting the embayment and the open ocean where large horizontal gradient of SPM transport occurs. This particular geomorphic setting results in a convergence of sediment transport toward the front of the river delta especially in wet season as a compound effect of summer monsoon, tides and enhanced river discharge.

Second, two distinct seasonal transport patterns, characterized by westward and offshore transport from the local rivers along SW Hainan, the eastern Hainan and the connected mainland coast in dry season, and by southward transport of the converged sediment plumes from the Red River and local rivers in SW Hainan in wet season, represent the dominant source-to-sink transport pathways for morphogenesis of the paleo-river delta. Typhoons play an important role in sediment redistribution in the study area and filling of the Yinggehai Basin, but is not the formation mechanism of the paleo-river delta.

Last but not least, the local rivers of Hainan are indicated as the main sediment supplier of the paleo-delta, despite that their discharge rate is much less than that of the Red River. In dry season, sediment from the Red River is mainly transported along the western coast of the embayment and detoured around the paleo-river delta, whilst in wet season most of the Red River-borne sediment is initially accumulated near the river mouth, with only a small portion transported towards the SW Hainan coast and converged with the local river sediment plume. This converged plume effectively feeds the development of the paleo-delta. However, further research is needed to address several knowledge gaps left still, especially an inconsistency in the sediment budget.

6. Data availability

Field data derived from the ERES project are available upon request from jan.harff@io-warnemuende.de. Numerical modeling data for this study are available upon request from wenyan.zhang@hzg.de.

Acknowledgements

This study is supported by the international research project ERES (NCN-ID: 2016/21/B/ST10/02939) and the research programme “Marine, Coastal and Polar Systems” (PACES II) of the Hermann von Helmholtz-Gemeinschaft Deutscher Forschungszentren e.V. It receives further support from the open fund of State Key Laboratory of Satellite Ocean Environment Dynamics, Second Institute of Oceanography, MNR(No. QNHX1819, No. SOEDZZ1905), the scientific research fund of the Second Institute of Oceanography, MNR (No. JG1811). The numerical simulations were done in the high-performance computer "Mistral" at German Climate Computing Center (DKRZ) in Hamburg.

References

An, Z., 2000. The history and variability of the East Asian paleomonsoon climate. Quaternary Science Reviews 19 (1-5), 171-187.

Anthony, E.J., 2015.Wave influence in the construction, shaping and destruction of river deltas: a review. Mar. Geol. 361, 53–78

Besset, M., Anthony, E.J., Bouchette, F., 2019. Multi-decadal variations in delta shorelines and their relationship to river sediment supply: An assessment and review. Earth-Science Reviews 193, 199–219.

Blum, M.D., Roberts, H.H., 2012. The Mississippi Delta Region: Past, Present, and Future. Annual Review of Earth and Planetary Sciences 40 (1), 655–683. doi:10.1146/annurev-earth-042711-105248

Blumberg, A.F., Mellor, G.L., 1987. A description of a three-dimensional coastal ocean circulation model. In: Heaps, N.S. (Ed.), Three-Dimensional Coastal Ocean Models. American Geophysical Union, Washington, DC, pp. 1–16.

Chen, H., J. Harff, Y. Qiu, A. Osadczuk, J. Zhang, M. Tomczak, Z. Cui, G. Cai, M. Wen, L. Li, 2016a. Last Glacial Cycle and seismic stratigraphic sequences offshore western Hainan Island, NW South China Sea: Geological Society, London, Special Publications, 429, 99-12.

Chen, H., Xie, X., Zhang, W., Shu, Y., Wang, D., Van Rooij, D., Vandorpe, T., 2016b. Deep-water sedimentary systems and their relationship with bottom currents at the intersection of Xi'sha Trough and Northwest Sub-Basin, South China Sea. Marine Geology, 378, 100-113. doi:10.1016/j.margeo.2015.11.002

Chen, H., Zhang, W., Xie, X., Ren, J. 2019. Sediment dynamics driven by contour currents and mesoscale eddies along continental slope: A case study of the northern South China Sea. Marine Geology, Volume 409, Pages 48-66, doi:10.1016/j.margeo.2018.12.012

Clift, P. D., Z. Sun, 2006, The sedimentary and tectonic evolution of the Yinggehai-Song Hong basin and the southern Hainan margin, South China Sea: Implications for Tibetan uplift and monsoon intensification: Journal of Geophysical Research, 111, B06405.

Clift, P. D., Wan, S. M., Blusztajn, J., 2014. Reconstructing chemical weathering, physical erosion and monsoon intensity since 25 Ma in the northern South China Sea: A review of competing proxies. Earth-Science Reviews 130, 86– 102.

Committee of Encyclopedia of Hainan, 1999. Encyclopedia of Hainan Island. China Press for Encyclopedia, Beijing, 893 pp (in Chinese).

Dang, T.H., Coynel, A., Orange, D., Blanc, G., Etcheber, H., Le L. A., 2010. Long-term monitoring (1960–2008) of the river-sediment transport in the Red River Watershed (Vietnam): temporal variability and dam-reservoir impact. Sci. Total Environ. 408 (20), 4654–4664.

Egbert, G.D., Erofeeva, L., 2002. Efficient inverse modeling of barotropic ocean tides. J. Atmos. Ocean. Technol. 19, 183–204.

Feng, Y., Zhan, W., Chen, H., Jiang, T., Zhang, J., Osadczuk, A., Yao, Y., Li, W., Sun, J., Guo, L., Huang, W., Li, S., Zhang, W., 2018. Seismic characteristics and sedimentary record of the late Pleistocene delta offshore south-western Hainan Island, north-western South China Sea. SEG, Interpretation 6(4), SO31-SO43. doi:10.1190/int-2018-0012.1

Galloway, W. E., 1975. Process framework for describing the morphologic and stratigraphic evolution of delta depositional systems. In: Broussard, M.L (Ed.), Deltas: Models for Exploration. Houston Geological Society, Houston, pp. 87–98.

Gan, J., Li, H., Curschitser, E. N., Haidvogel, D. B., 2006. Modeling South China Sea circulation: response to seasonal forcing regimes. Journal of Geophysical Research 111, C06034. doi: 10.1029/2005JC003298

Geleynse, N., Storms, J.E.A., Walstra, D.J.R., Jagers, H.R.A., Wang, Z.B., Stive, M.J.F., 2011.Controls on river delta formation; insights from numerical modeling. Earth and Planetary Science Letters 302, 217–226.

Hanebuth, T.J.J., Zhang, W., Hofmann, A.L., Löwemark, L.A., Schwenk, T., 2015. Oceanic density fronts steering bottom-current induced sedimentation deduced from a 50 ka contourite-drift record and numerical modeling (off NW Spain). Quat. Sci. Rev. 112, 207–225.

Hoitink, A. J. F., Wang, Z. B., Vermeulen, B., Huismans, Y., Kästner, K., 2017. Tidal controls on river delta morphology. Nature Geoscience, 10(9), 637– 645. doi: 10.1038/ngeo3000

Hu, J., H. Kawamura, D. Tang, 2003. Tidal front around the Hainan Island, northwest of the South China Sea. Journal of Geophysical Research, 108, C11, 3342

HydroQual, Inc., 2002. A Primer for ECOMSED Version 1. 3. (Computer Program Manual), Mahwah, N. J.

Li, G., Zhou, L., Qi, Y., Gao, S., 2019. Threshold sediment flux for the formation of river deltas in Hainan Island, southern China. Journal of Geographical Sciences 29(1), 146-160. doi: 10.1007/s11442-019-1589-y

Li, M., Ouyang, T., Tian, C., Zhu, Z., Peng, S., Tang, Z., Qiu, Y., Zhong, H., Peng, X., 2019. Sedimentary responses to the East Asian monsoon and sea level variations recorded in the northern South China Sea over the past 36 kyr. Journal of Asian Earth Sciences 171, 213-224.

Li, S., Dai, Z., Mei, X., Huang, H., Wei, W., Gao, J., 2017. Dramatic variations in water discharge and sediment load from Nanliu River (China) to the Beibu Gulf during 1960s-2013. Quaternary International 440 (A), 12-23.

Liu, J., Steinke, S., Vogt, C., Mohtadi, M., De Pol-Holz, R., Hebbeln, D., 2017. Temporal and spatial patterns of sediment deposition in the northern South China Sea over the last 50,000 years. Palaeogeography, Palaeoclimatology, Palaeoecology 465 (A), 212-224.

Liu, Q., Kaneko, A., Su, J., 2008. Recent progress in studies of the South China Sea circulation. Journal of Oceanography 64, 753-762.

Liu, Z., Colin, C., Li, X., Zho, Y., Tuo, S., Chen, Z., Siringan, F. P., Liu, J. T., Huang, C., You, C., Huang, K., 2010. Clay mineral distribution in surface sediments of the northeastern South China Sea and surrounding fluvial drainage basins: source and transport. Marine Geology 277, 48-60.

Luu, T. N. M., Garnier, J., Billen, G., Orange, D., Némery, J., Le, T.P.Q., Tran, H. T., Le, L.A., 2010. Hydrological regime and water budget of the Red River Delta (Northern Vietnam). J Asian Earth Sci 37:219–28.

McCalpin, J., 1994. A comparison of second-order and fourth-order pressure gradient algorithms in a s-coordinate ocean model. Int. J. Numer. Meth. Fluids, 18, 361– 383.

Mellor, G.L., 2003. Users Guide for a Three-Dimensional, Primitive Equation, Numerical Ocean Model. Atmospheric and Oceanic Sciences Princeton University.

Milliman, J. D., Farnsworth, K. L., 2011. River discharge to the coastal ocean—A global synthesis. NY: Cambridge University Press.

Miluch, J., Osadczuk A., Chen H., Feldens P., Harff J., Maciąg Ł., submitted. Geometry and sedimentary architecture of the late Pleistocene delta in the Beibu Gulf, SW of Hainan Island, based on the seismic profiles. Journal of Asian Earth Sciences, this issue.

Miramontes, E., Garreau, P., Caillaud, M., Jouet, G., Pellen, R., Hernández-Molina, F. J., Clare, M. A., Cattaneo, A., 2019b. Contourite distribution and bottom currents in the NW Mediterranean Sea: coupling seafloor geomorphology and hydrodynamic modelling. Geomorphology 333: 43– 60.

Orton, G.J., Reading, H.G., 1993. Variability of deltaic processes in terms of sediment supply, with particular emphasis on grain size. Sedimentology 40 (3), 475–512

Styles, R., Glenn, S. M., 2000. Modeling stratified wave and current bottom boundary layers on the continental shelf. J. Geophys. Res. 105(C10), 24,119–24,139.

Sündermann, J., Pohlmann, T., 2011. A brief analysis of North Sea physics. Oceanologia, 53(3), 663–689. https://doi.org/10.5697/oc.53–3.663

Swenson, J.B., Paola, C., Pratson, L., Voller, V.R., Murray, A.B., 2005. Fluvial and marine controls on combined subaerial and subaqueous delta progradation: morphodynamic modeling of compound-clinoform development. J. Geophys. Res. 110 (F02013)

Tomczak, M., Kaiser, J., Zhang, J., Arz, H.W., Voss, M., Witkowski, A., etc., submitted. Monsoon and ocean circulation controls on paleo-environmental conditions off the SW Hainan Island during the last glacial period. Journal of Asian Earth Sciences, this issue.

Waelbroeck, C., L. Labeyrie, E. Michel, J. C. Duplessy, J. F. McManus, K. Lambeck, E. Balbon, Labracherie, M., 2002. Sea-level and deep water temperature changes derived from benthic foraminifera isotopic records. Quaternary Science Reviews 21, 295-305. doi: 10.1016/S0277-3791(01)00101-9

Wang, X., Ma, D., Jiang, D., 1991. Geology of Hainan Island (II): Tectonic Geology. Beijing: Geological Press, 1-106 (in Chinese).

Wang, Y., Peter, M.I., Zhu, D., Zhang, Y., Tang, W., 2001. Coastal plain evolution in southern Hainan Island, China. Chinese Science Bulletin, 46(1): 90–96.

Wu, C.Y., Wei X., Ren, J., Bao, Y., He, Z.G., Lei, Y.P., Shi, H.Y., and Zhang, W., 2010. Morphodynamics of the rock-bound outlets of the Pearl River estuary, South China – A preliminary study. Journal of Marine Systems, 82(1), 17- 27. doi:10.1016/j.jmarsys.2010.02.002

Xiong, P., Dudzinska-Nowak, J., Harff, J., Xie, X., Zhang, W., Chen, H., Jiang, T., Chen, H., Miluch, J., Feldens, P., Maciag, L., Osadczuk, A., Meng, Q., Zorita, E., submitted. Paleogeographic scenarios of northwestern shelf of the South China Sea during the last glacial cycle. Journal of Asian Earth Sciences, this issue.

Xue, C.T., 1993. Historical changes in the Yellow River delta, China. Mar. Geol. 113, 321–329.

Yang, Z., Jia, J., Wang, X., Gao, J., 2013. Characteristics and variations of water and sediment fluxes into the sea of the top three rivers of Hainan in recent 50 years. Marine Science Bulletin 32(1), 92–99. (in Chinese with English abstract)

Yin, S., Hernandez-Molina, F. J., Zhang, W., Li, j., Wang, L., Ding, W., Ding, W., 2019. The influence of oceanographic processes on contourite features: a multidisciplinary study of the northern South China Sea. Marine Geology, doi: 10.1016/j.margeo.2019.105967

Zhang, J., Wang, D., Jennerjahn, T., Dsikowitzky, L., 2013. Land-sea interactions at the east coast of Hainan Island, South China Sea: a synthesis. Continental Shelf Research, 57: 132–142

Zhang, W., Harff, J., Schneider, R., Wu, C.Y., 2010. Development of a modeling methodology for simulation of long-term morphological evolution of the southern Baltic coast. Ocean Dynamics 60, 1085–1114.

Zhang, W., Harff, J., Schneider, R., Meyer, M., Wu, C.Y., 2011. A multi-scale centennial morphodynamic model for the southern Baltic coast. Journal of Coastal Research 27, 890-917. doi:10.2112/JCOASTRES-D-10-00055.1

Zhang, W., Schneider, R., Harff, J., 2012. A multi-scale hybrid long-term morphodynamic model for wave-dominated coasts. Geomorphology 149-150, 49-61. doi:10.1016/j.geomorph.2012.01.019

Zhang, W., Harff, J., Schneider, R., Meyer, M., Zorita, E., Hünicke, B., 2014. Holocene morphogenesis at the southern Baltic Sea: simulation of multiscale processes and their interactions for the Darss-Zingst peninsula. Journal of Marine Systems 129, 4-18. doi:10.1016/j.jmarsys.2013.06.003

Zhang, W., Cui, Y., Santos, A. I. Hanebuth, T. J. J., 2016. Storm-driven bottom sediment transport on a high-energy narrow shelf (NW Iberia) and development of mud depocenters. Journal of Geophysical Research: Oceans, 121, 5751–5772. doi:10.1002/2015jc011526

Zhang, W., Wirtz, K., Daewel, U., Wrede, A., Kröncke, I., Kuhn, G., Neumann, A., Meyer, J., Ma, M., Schrum, C., 2019. The budget of macrobenthic reworked organic carbon - a modelling case study of the North Sea. Journal of Geophysical Research-Biogeosciences, doi:10.1029/2019JG005109.

Figures:

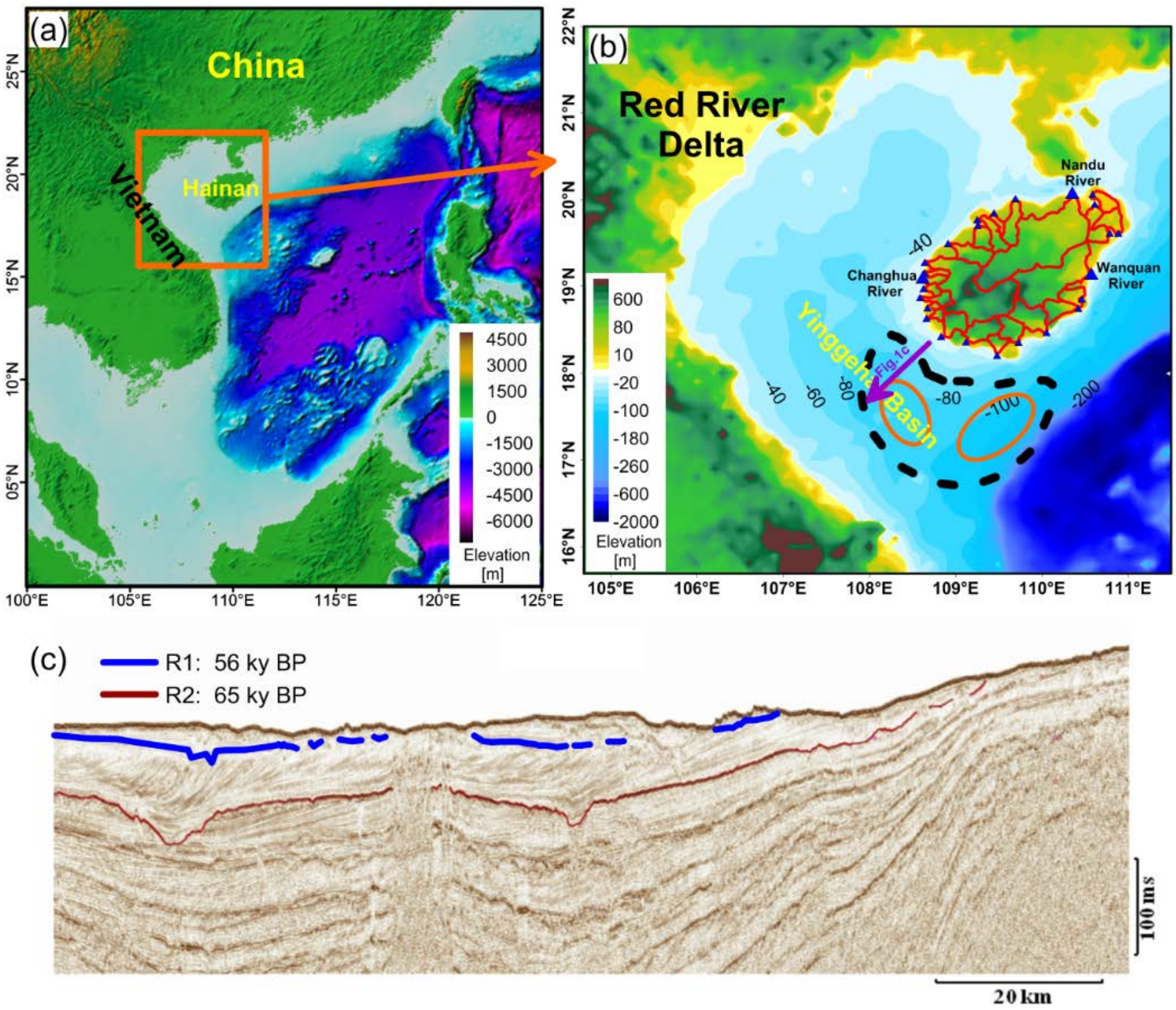

Figure 1. (a) Digital Elevation Model (DEM) of the South China Sea based on the GEBCO database (GEBCO_2014, v. 2014-11-03, http://www.gebco.net) and location of our local study area. (b) Modern DEM of the local study area. Location of the paleo-delta is indicated by the dashed frame. Two locally confined depocenters (thickness larger than 50 m) of the delta are indicated by the ellipses**,** with details of sediment isopach shown in Figure 2. The depth contours on the coastal shelf are marked by numbers. Red solid lines on the Hainan Island indicate catchment basins and triangles indicate existing major river mouths over the island, with the top three rivers (Nandu, Changhua and Wanquan) marked in larger size. (c) Seismic profile across the paleo-delta, with its location marked by the arrow in (b). R2 and R1 in (c) mark the surfaces of initialization and termination of the delta, respectively (Feng et al., 2018).

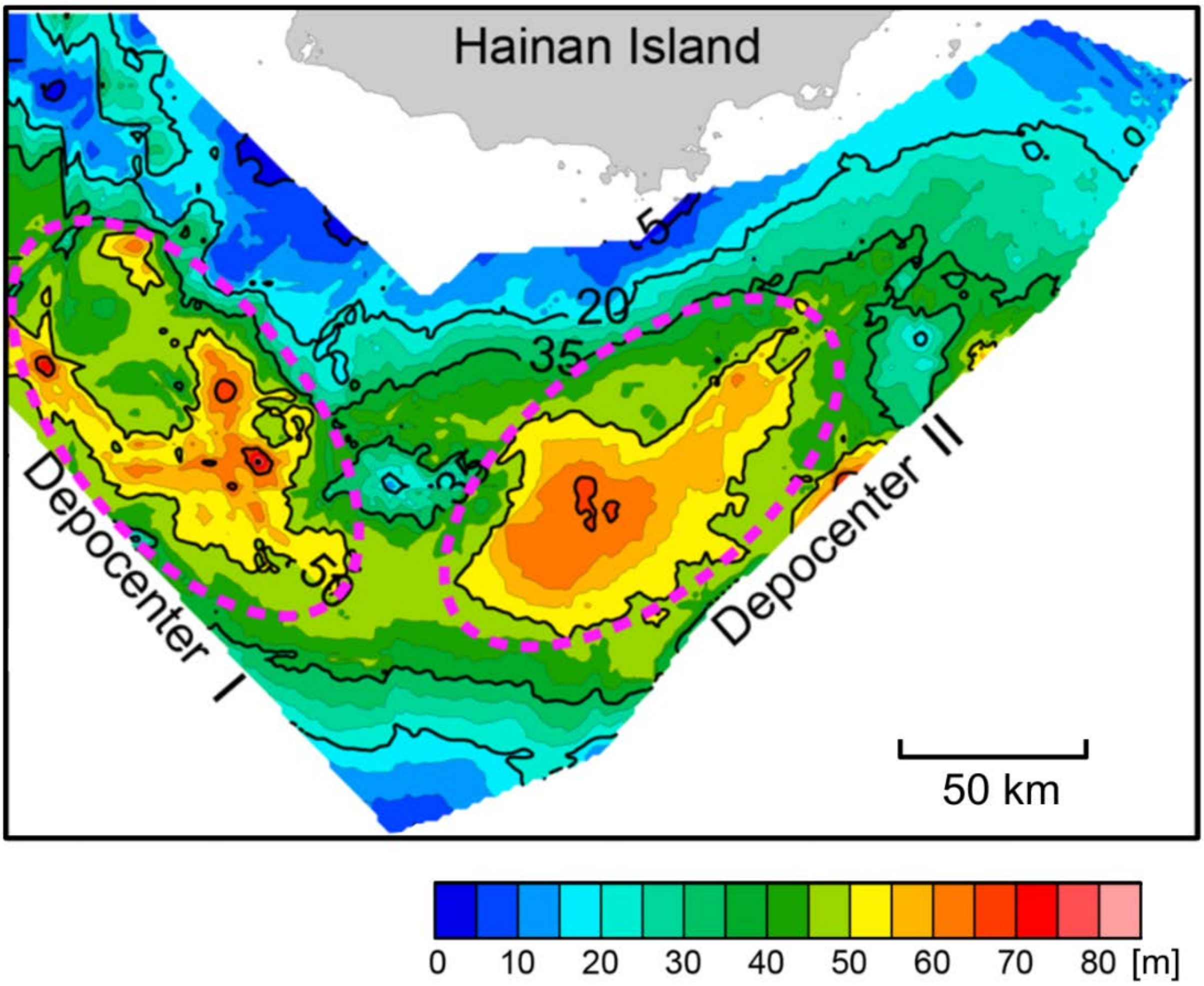

Figure 2. Sediment isopach map of the paleo-river delta deposit modified from Feng et al.(2018).

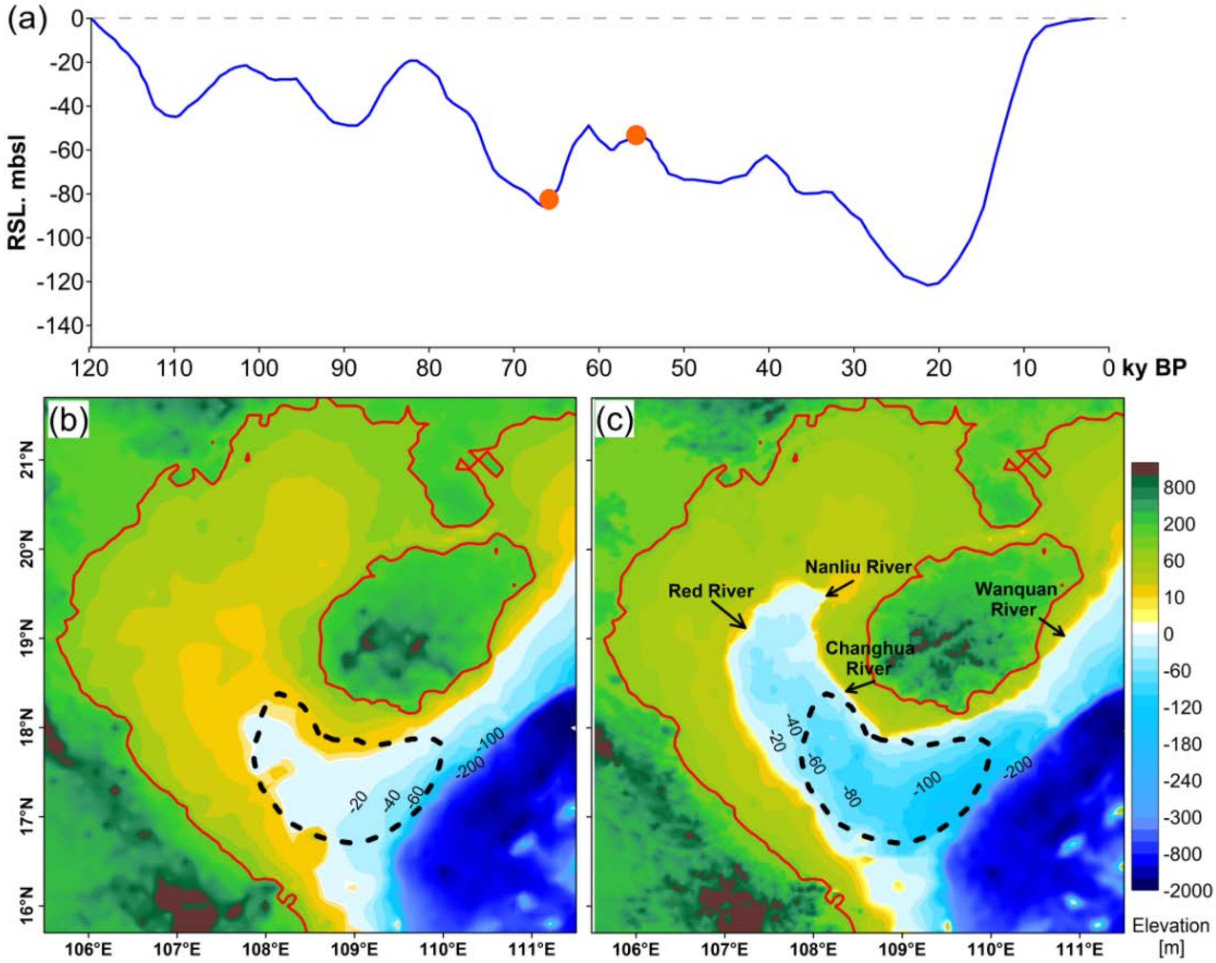

Figure 3. Global mean sea level curve (a) after Waelbroeck et al. (2002) with initialization and termination of the paleo-delta development marked by circles, respectively, and two-step reconstruction (b & c) of the Paleo-DEM of the study area in 65 kyr BP. (b) Step 1–Reversal of the eustatic sea level by 85 m from the modern sea level; (c) Step 2–Removal of the sediment deposit layer after 65 kyr BP (backstripping). The modern coastline is marked by the red solid line. The paleo-river mouth of four major rivers considered in modeling are indicated by arrows. Location of the paleo-delta is indicated by the dashed frame. The depth contours on the coastal shelf are marked by numbers.

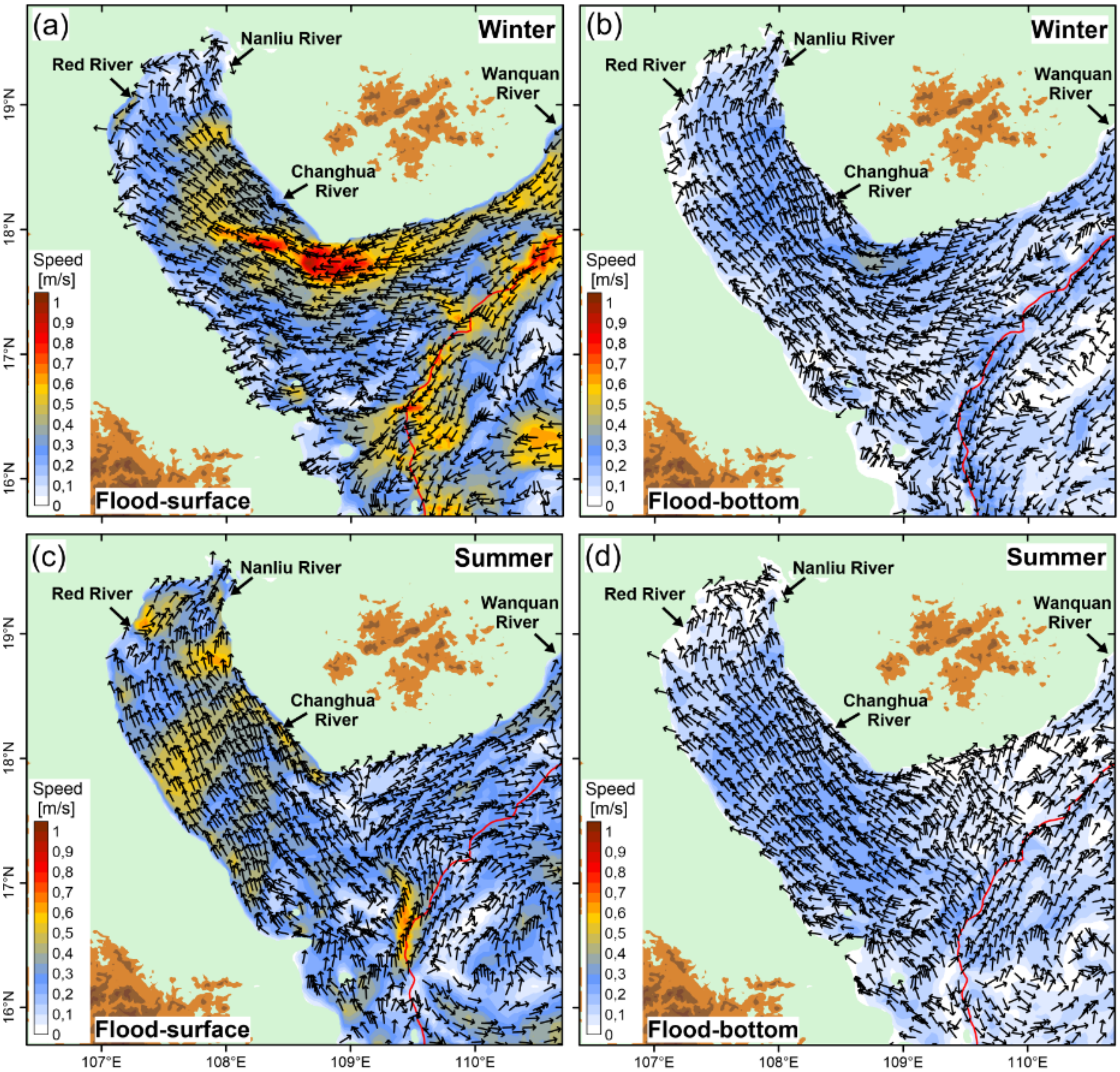

Figure 4. Flood tidal currents in the study area in two distinct seasons affected by the monsoon. The arrows indicate flow directions, with flow strength plotted in colour. Vectors are plotted over fifteen grid cells in both x and y directions. The 200 m water depth contour marking the shelf break is shown by the red solid line.

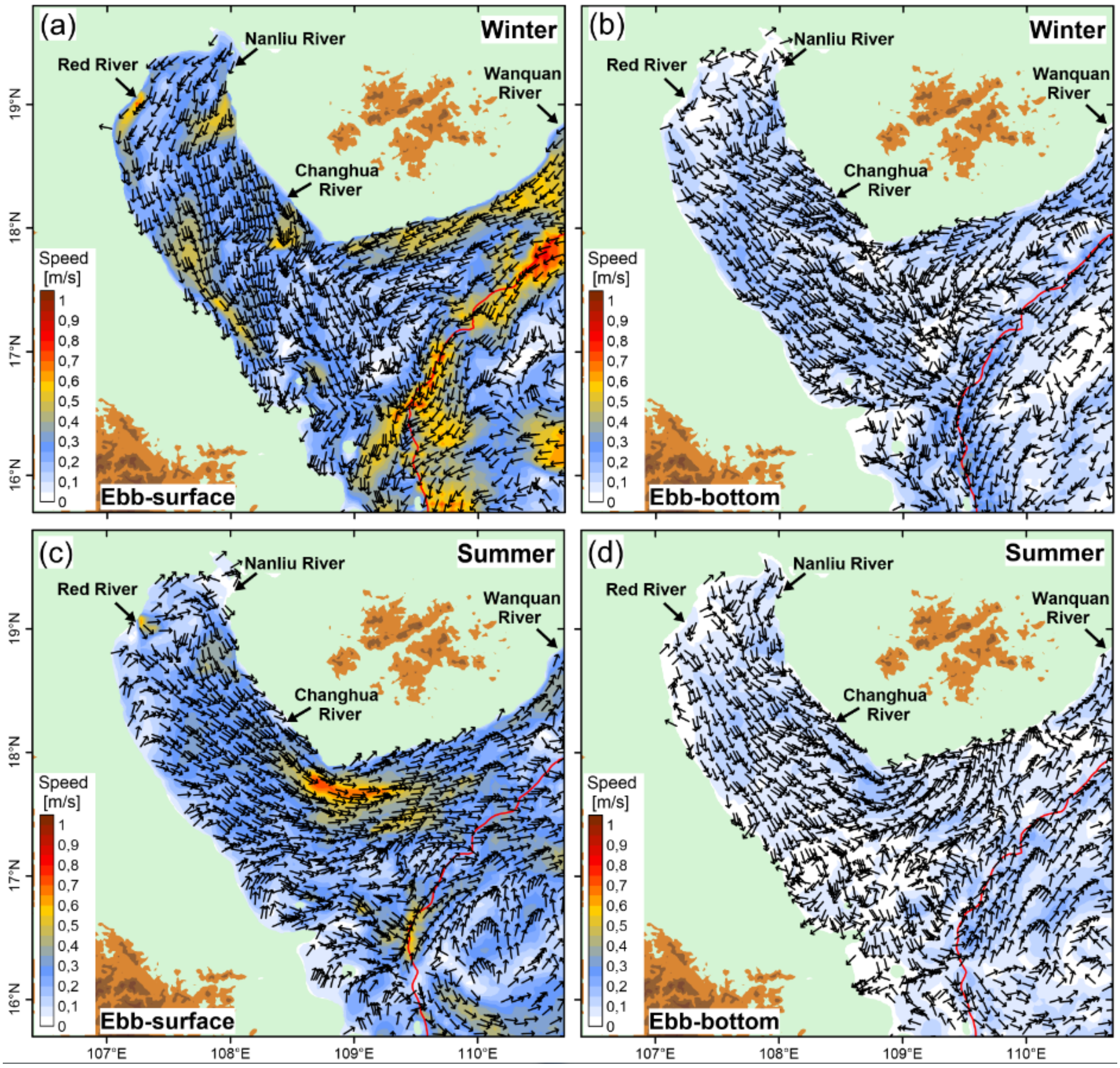

Figure 5. Similar to Figure 4 but for the ebb tidal currents.

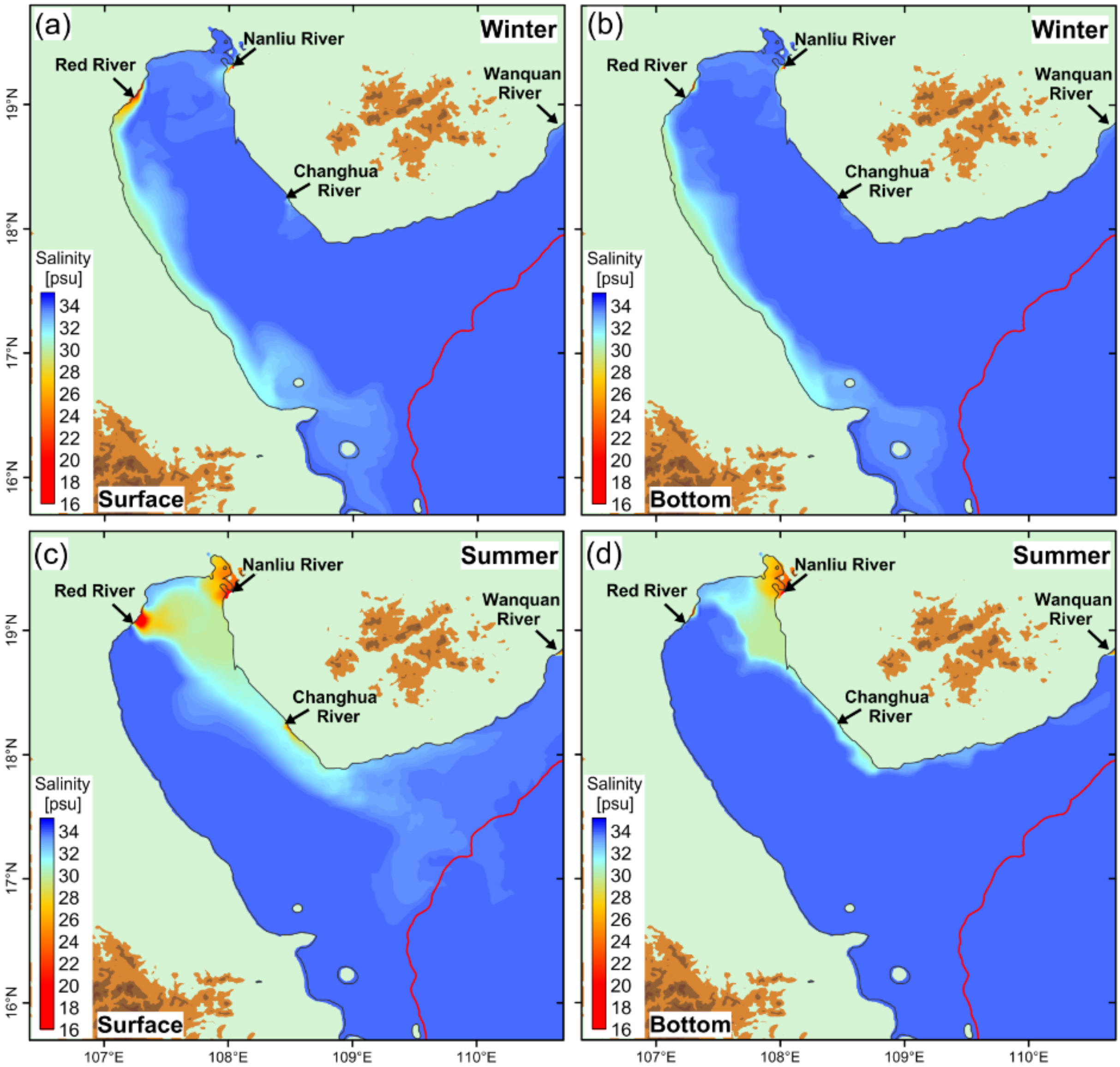

Figure 6. Distribution of surface and bottom water salinity in the study area in two distinct seasons driven by the monsoon. The 200 m water depth contour marking the shelf break is shown by the red solid line.

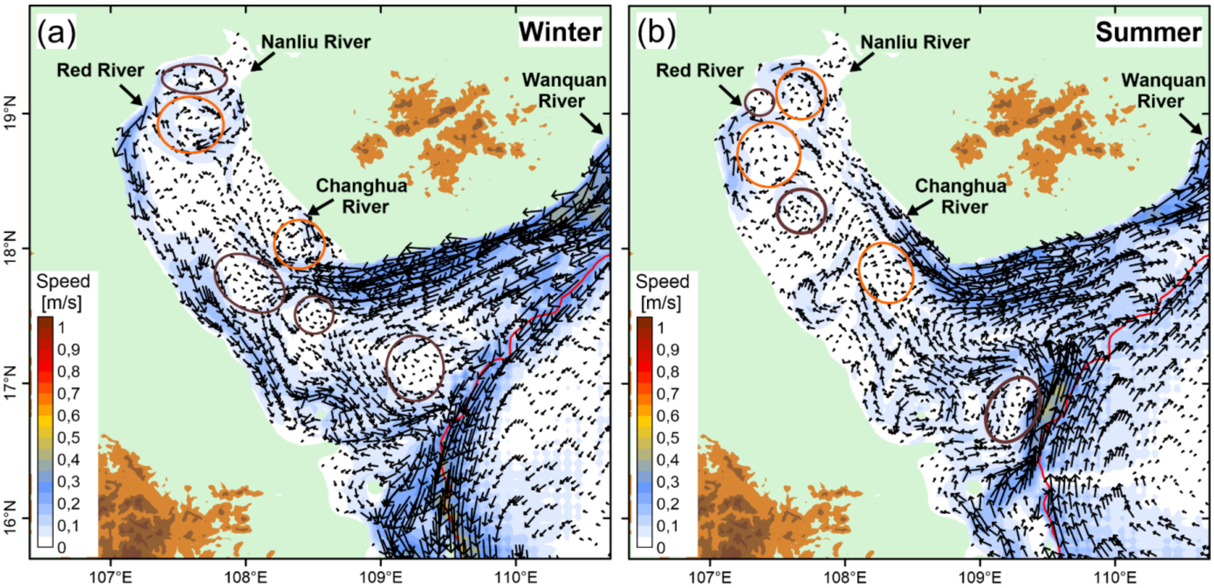

Figure 7. Residual currents in the study area in two distinct seasons driven by the monsoon and tides. The arrows indicate flow vectors, with vertically-averaged current strength plotted in colour. The ellipses in orange and brown colour indicate anti-cyclonic and cyclonic gyres, respectively. Vectors are plotted over four grid cells in both x and y directions. The 200 m water depth contour marking the shelf break is shown by the red solid line.

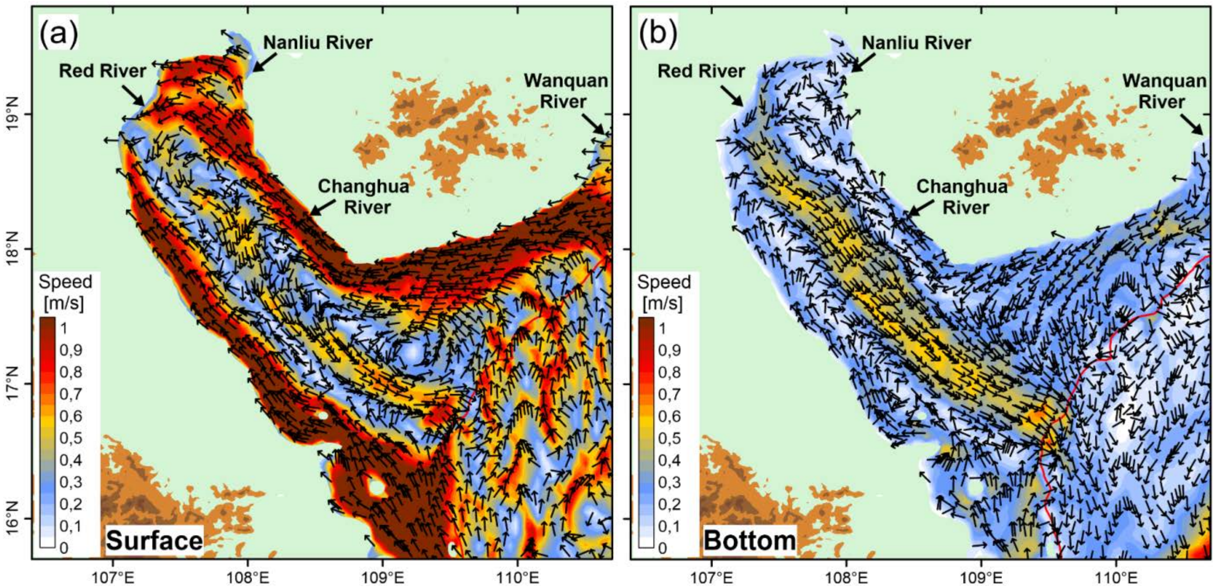

Figure 8. Similar to Figure 4 but for currents during typhoon.

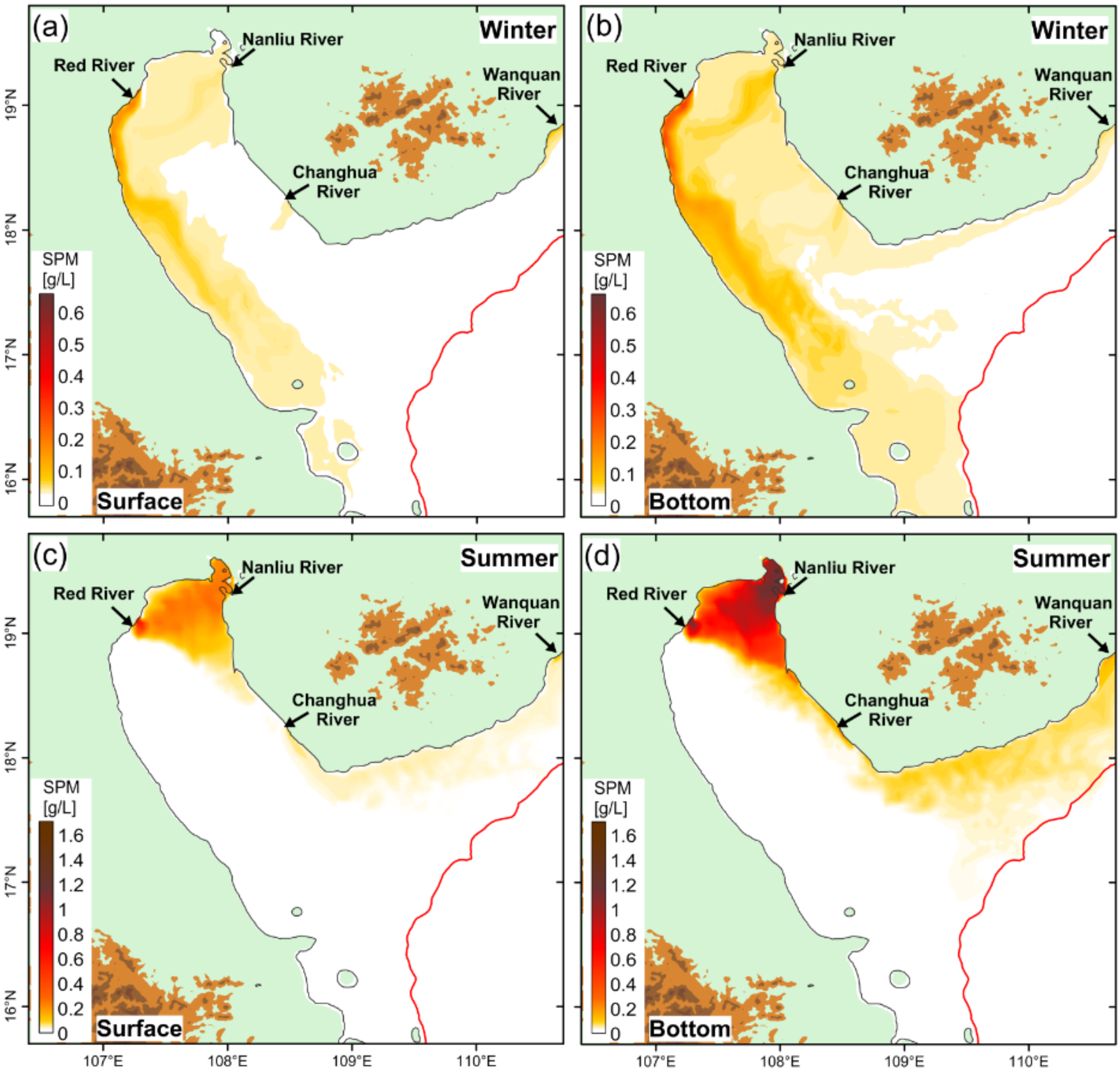

Figure 9. Similar to Figure 5 but for the suspended sediment concentration. Note that the colour bar is different between winter and summer.

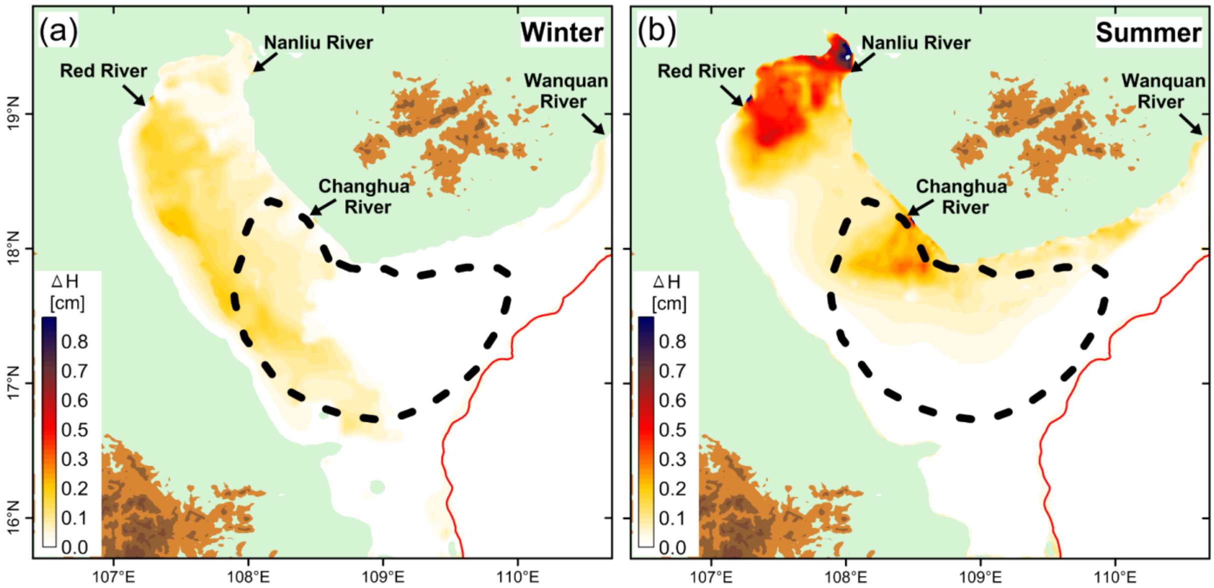

Figure 10. Simulated river-borne sediment deposition in the study area in two distinct seasons driven by the monsoon and tides.

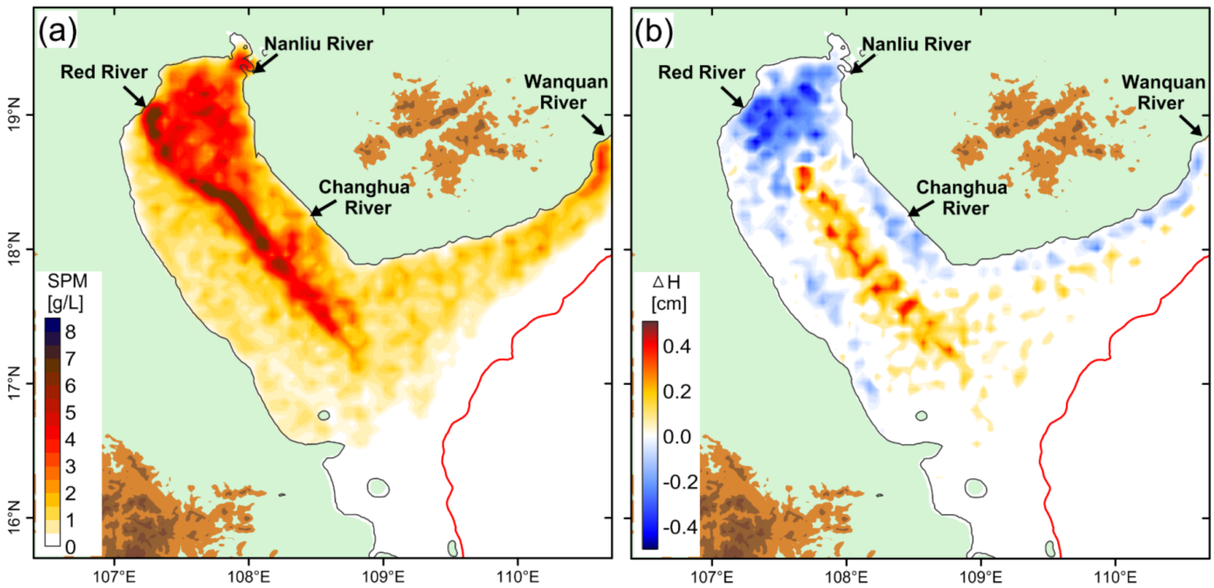

Figure 11. (a) Simulated suspended sediment concentration near the bottom during the typhoon, and (b) bed level change after the typhoon.

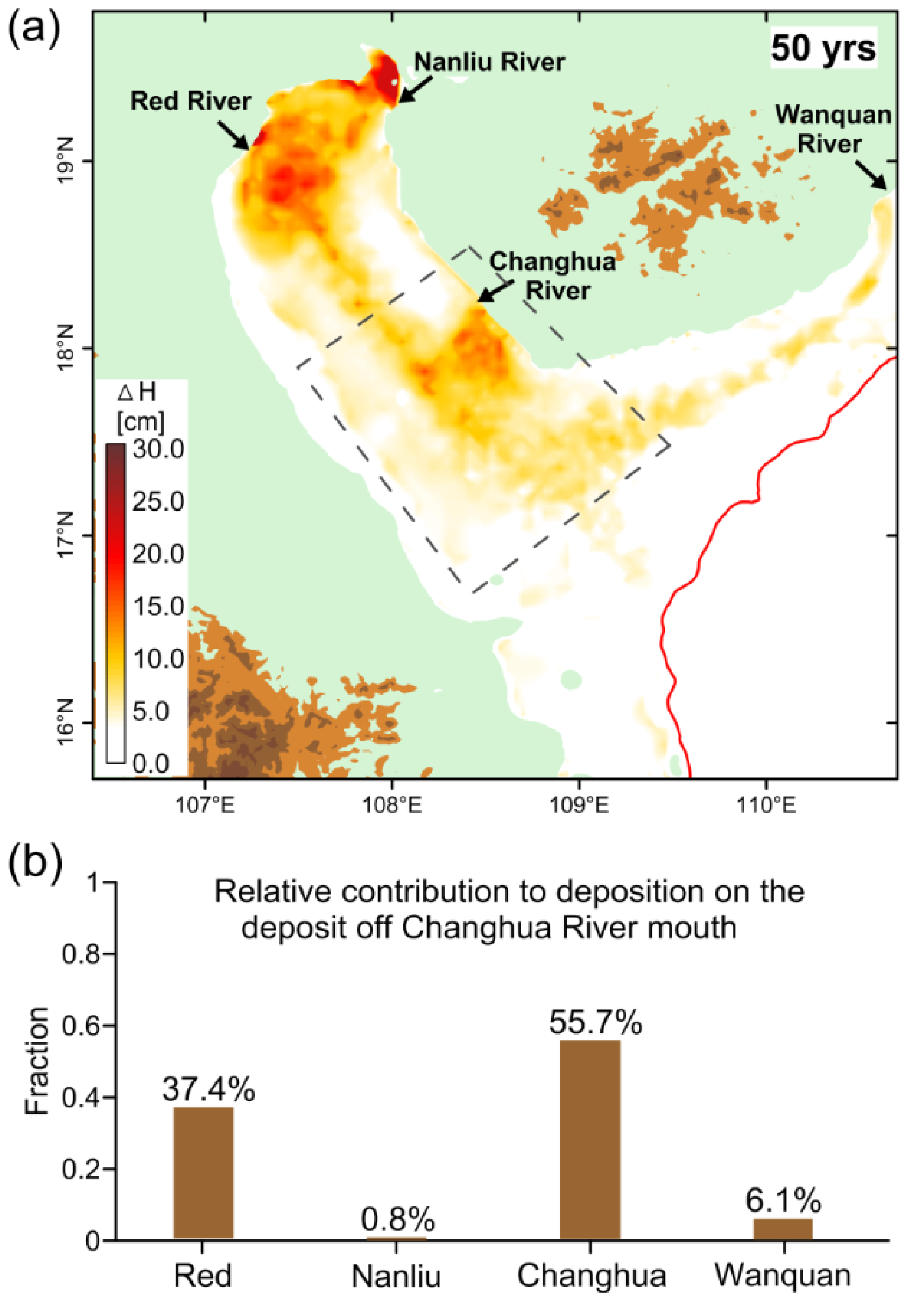

Figure 12. (a) Simulated river-borne sediment deposition after 50 yrs; (b) Contribution of each river to the sediment budget of the deposit off Changhua River mouth. The area of calculation is indicated by the dashed frame in (a).

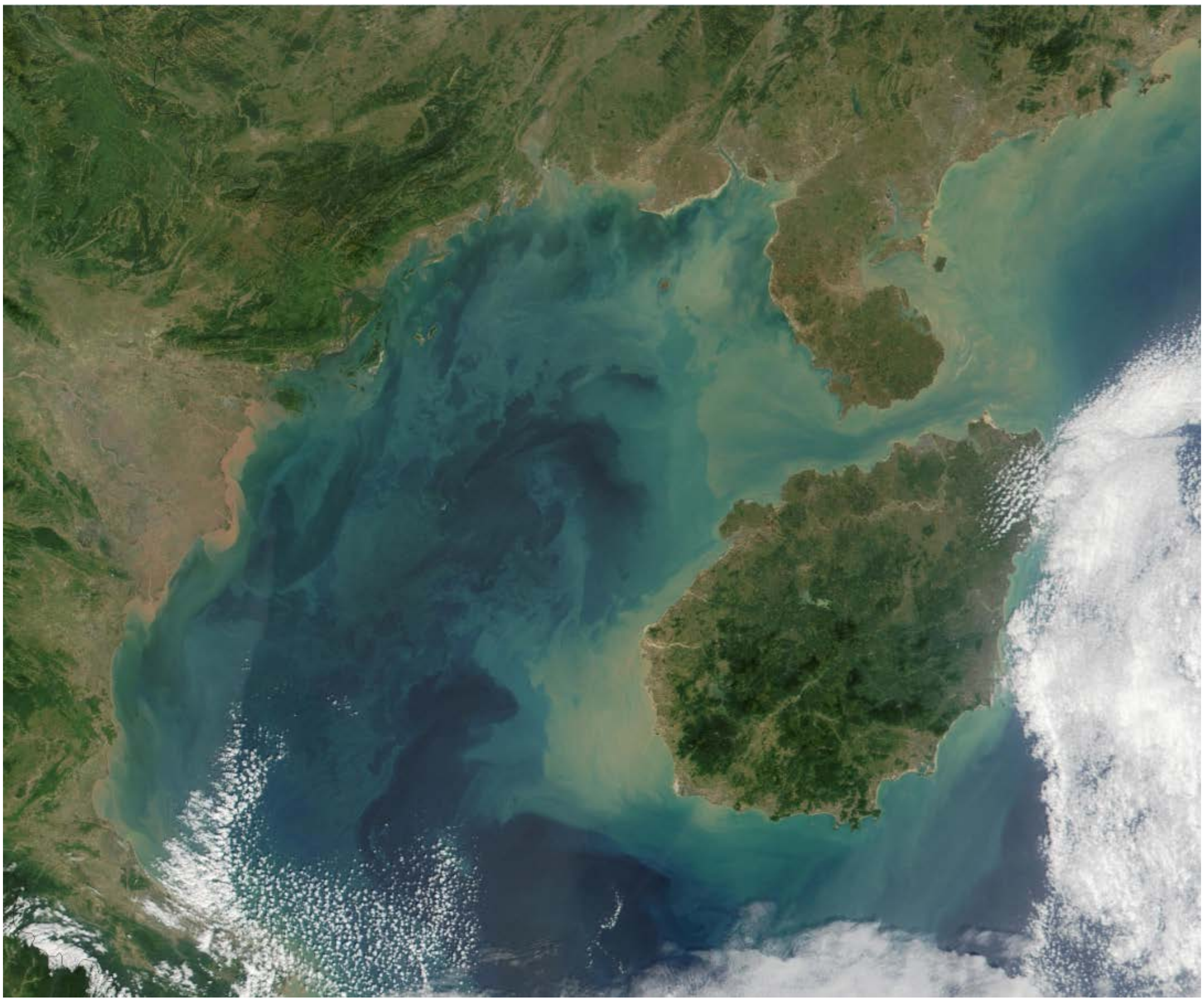

Figure 13. True-color satellite image captured by MODIS in November 2001 showing remarkable turbid water along the SW Hainan coast. Image source: NASA.